



RESEARCH ARTICLE

WILEY

Hybrid scaffolds of Mg alloy mesh reinforced polymer/extracellular matrix composite for critical-sized calvarial defect reconstruction

Yingqi Chen^{1,2} | Sang-Ho Ye¹ | Hideyoshi Sato¹ | Yang Zhu¹ | Vesselin Shanov³ | Tarannum Tiasha³ | Antonio D'Amore¹ | Samuel Luketich¹ | Guojiang Wan² | William R. Wagner^{1,4,5,6}

¹McGowan Institute for Regenerative Medicine, University of Pittsburgh, Pittsburgh, PA, USA

²Key Laboratory of Advanced Technologies of Materials, Ministry of Education, College of Materials Science and Engineering, Southwest Jiaotong University, Chengdu, China

³College of Engineering and Applied Science, University of Cincinnati, Cincinnati, OH, USA

⁴Department of Surgery, University of Pittsburgh, Pittsburgh, PA, USA

⁵Department of Chemical Engineering, University of Pittsburgh, Pittsburgh, PA, USA

⁶Department of Bioengineering, University of Pittsburgh, Pittsburgh, PA, USA

Correspondence

William R. Wagner, McGowan Institute for Regenerative Medicine, University of Pittsburgh, Pittsburgh, PA 15219, USA. Email: wagnerwr@upmc.edu

Gujiang Wan, Key Laboratory of Advanced Technologies of Materials, Ministry of Education, College of Materials Science and Engineering, Southwest Jiaotong University, Chengdu 610031, China. Email: guojiang.wan@home.swjtu.edu.cn; superwgj@263.net

Funding information

China Scholarship Council, Grant/Award Number: 201507000009; Education Program for Innovation & Entrepreneurship for Southwest Jiaotong University; Sichuan Youth Science & Technology Foundation, Grant/Award Number: 2012JQ0001; National Key R&D Program of China, Grant/Award Number: 2016YFC1102500; National Natural Science Foundation of China, Grant/Award Number: 21473138; U.S. National Science Foundation, Grant/Award Number: Award NSF 0812348

Abstract

The challenge of developing scaffolds to reconstruct critical-sized calvarial defects without the addition of high levels of exogenous growth factor remains relevant. Both osteogenic regenerative efficacy and suitable mechanical properties for the temporary scaffold system are of importance. In this study, a Mg alloy mesh reinforced polymer/demineralized bone matrix (DBM) hybrid scaffold was designed where the hybrid scaffold was fabricated by a concurrent electrospinning/electrospraying of poly(lactic-co-glycolic acid) (PLGA) polymer and DBM suspended in hyaluronic acid (HA). The Mg alloy mesh significantly increased the flexural strength and modulus of PLGA/DBM hybrid scaffold. In vitro results demonstrated that the Mg alloy mesh reinforced PLGA/DBM hybrid scaffold (Mg-PLGA@HA&DBM) exhibited a stronger ability to promote the proliferation of bone marrow stem cells (BMSCs) and induce BMSC osteogenic differentiation compared with control scaffolding materials lacking critical components. In vivo osteogenesis studies were performed in a rat critical-sized calvarial defect model and incorporated a variety of histological stains and immunohistochemical staining of osteocalcin. At 12 weeks, the rat model data showed that the degree of bone repair for the Mg-PLGA@HA&DBM scaffold was significantly greater than for those scaffolds lacking one or more of the principal components. Although complete defect filling was not achieved, the improved mechanical properties, promotion of BMSC proliferation and induction of BMSC osteogenic differentiation, and improved promotion of bone repair in the rat critical-sized calvarial defect model make Mg alloy mesh reinforced PLGA/DBM hybrid scaffold an attractive option for the repair of critical-sized bone defects where the addition of exogenous isolated growth factors is not employed.

KEYWORDS

biodegradable Mg alloy, bone regeneration, critical-sized bone defect, electrospinning/electrospraying, mechanical property, osteogenic differentiation

1 | INTRODUCTION

Critical-sized bone defects, those that cannot be repaired without externally derived factors, may result from trauma, primary tumours, congenital diseases, and other causes (Hokugo et al., 2004). The repair of critical-sized calvarial defects remains challenging in terms of achieving adequate osteogenic regenerative efficacy and reaching suitable mechanical properties (Cuthbert et al., 2013; Dimitriou, Mataliotakis, Calori, & Giannoudis, 2012). Common approaches applied to regenerate bone in this setting include autologous bone grafting and the use of alloplastic implants, but both techniques have disadvantages (Amini, Laurencin, & Nukavarapu, 2012). Autologous tissue is subject to limited availability, donor site morbidity, and infection risk. Allografts bring risks for immunoreactivity and the transmission of infectious agents (Amini et al., 2012; Henkel et al., 2013). Alternatively, bone tissue engineering approaches based on scaffolds have shown promise in the repair of large bone defects.

A broad variety of scaffolds aimed at improving osteogenic regenerative capacity have been developed, including porous ceramics/bioactive glasses (e.g., calcium phosphate [Zhang et al., 2015], magnesium phosphate [Kim, Lim, Naren, Yun, & Park, 2016], and calcium silicate bioactive ceramics [El-Rashidy et al., 2017; Nommeots-Nomm et al., 2017]), membranes (multilayered graphene hydrogel composite membranes [Lu et al., 2016], nanocomposite membranes [Zhang, Zhang, et al., 2016], and others), hydrogels (nanosilver/nanosilica hydrogels [Zhang, Guo, et al., 2016; Zhang, Liu, et al., 2016; Zhang, Xu, et al., 2016; Zhang, Zhang, et al., 2016], chitin nanofibre/calcium phosphate hydrogels [Kawata et al., 2016], and chitosan/hydroxyapatite hybrid hydrogels [Li, Wang, et al., 2015]), composites (chitosan-copper scaffolds [D'Mello et al., 2015], porous polymer/hydroxyapatite composites [Fujihara, Kotaki, & Ramakrishna, 2005; Zhang, Guo, et al., 2016; Zhang, Liu, et al., 2016; Zhang, Xu, et al., 2016; Zhang, Zhang, et al., 2016]), nanofibrous scaffolds (Li, Chu, et al., 2015; Li, Wang, et al., 2015; Li, Zhou, et al., 2015; Zhu et al., 2017), and others (Inzana et al., 2014; Shi, Wang, et al., 2017; Seo, Koh, & Song, 2017). Among these options, nano/micro fibrous scaffolds are readily fabricated using electrospinning technology that has been explored extensively in the biomaterials literature over the past decade (Shin, Purevdorj, Castano, Planell, & Kim, 2012). The nano- to sub-micron fibre structure can provide topographical cues and a connective porous network, which is beneficial for promoting bone cell adhesion, proliferation, migration, and nutrient transfer (Holzwarth & Ma, 2011). Further, osteogenic differentiation can be induced from such scaffolds by adding bioactive particles or providing for the controlled release of pharmacologic agents.

From a biologically derived materials perspective, extracellular matrix (ECM)-based materials, such as demineralized bone matrix (DBM), are of great relevance as a bone healing material, possessing a variety of bioactive factors, but lacking the mechanical properties needed in load-bearing applications. DBM is generated from allograft bone that has been processed to remove most of the inorganic minerals, providing an organic collagen-rich matrix, including type I and some type IV and X collagens, growth factors (BMP-2 and BMP-7),

and other bioactive entities, which are known to facilitate osteoconduction and osteoinduction (Gruskin, Doll, Futrell, Schmitz, & Hollinger, 2012).

As a support material, magnesium-based alloys have shown great potential in bone repair applications in many preclinical and, more recently, clinical reports (Zhao et al., 2017). The attractiveness of these alloy systems is based on several features. Most obviously, such alloys can be designed to experience oxidation and complete degradation *in situ* (Witte, 2015), avoiding secondary removal surgeries and their associated costs and morbidities. Second, the oxidative products from Mg alloy degradation are generally safe (Dziuba et al., 2013) and common in bone. Indeed, the release of Mg ions can promote calcitonin gene-related polypeptide- α -mediated osteogenic differentiation, which can be of therapeutic value (Zhang, Guo, et al., 2016; Zhang, Liu, et al., 2016; Zhang, Xu, et al., 2016; Zhang, Zhang, et al., 2016). Third, the mechanical properties of Mg alloys, particularly Young's modulus, can be similar to cortical bone, helping to minimize stress shielding that occurs with stiffer metallic implants (Zheng et al., 2014). However, substantial advances must still be made for Mg-based materials to find routine use. The corrosion rate for many applications may be too rapid, leading to premature loss of mechanical properties and potentially the build-up of hydrogen gas pockets associated with the reduction reaction (Wang, Witte, et al., 2015). Many strategies are being reported in efforts to slow or delay the corrosion process, particularly surface modification and microstructure control (Agarwal, Curtin, Duffy, & Jaiswal, 2016; Willbold et al., 2015; Wu, Ibrahim, & Chu, 2013; Yu et al., 2013). Related to the investigation of Mg alloys as the basis for orthopaedic fixation devices, there have been more recent efforts to incorporate Mg alloy components that would work in concert with other degradable (or non-degradable) elements to facilitate better healing outcomes. These approaches leverage the bone-stimulating ability that has been recognized in association with Mg degradation (Li et al., 2017; Li, Chu, et al., 2015; Li, Wang, et al., 2015; Li, Zhou, et al., 2015; Shi, Pei, et al., 2017; Shi, Wang, et al., 2017; Wu, Ibrahim, et al., 2013; Wu, Li, et al., 2013).

In considering the design features desirable for a device intended to facilitate calvarial defect regeneration, the following properties are considered most salient: (a) biodegradability to avoid secondary surgeries, (b) suitable mechanical properties, especially bending stress and bending modulus matched with surrounding tissue to reduce stress and strain imbalances, and (c) bioactivity to promote bone cell adhesion, proliferation, migration, and secretion of ECM proteins for subsequent calcification. The objective of this study was to design a composite device to incorporate these features by leveraging a Mg alloy mesh for strength, form, and bioactivity, DBM for broad bioactive component incorporation, and poly(lactic-co-glycolic acid) (PLGA) as a binding matrix for DBM. This hybrid scaffold was fabricated by concurrent electrospinning/electrospraying of a PLGA polymer and DBM onto a Mg alloy mesh (Figure 1a). The mechanical properties, including flexural stress and modulus, *in vitro* osteogenic differentiation capacity, and *in vivo* osteogenesis in a rat calvarial defect model, were assessed for the designed scaffold system as well as for control scaffolds lacking key elements of the developed composite.

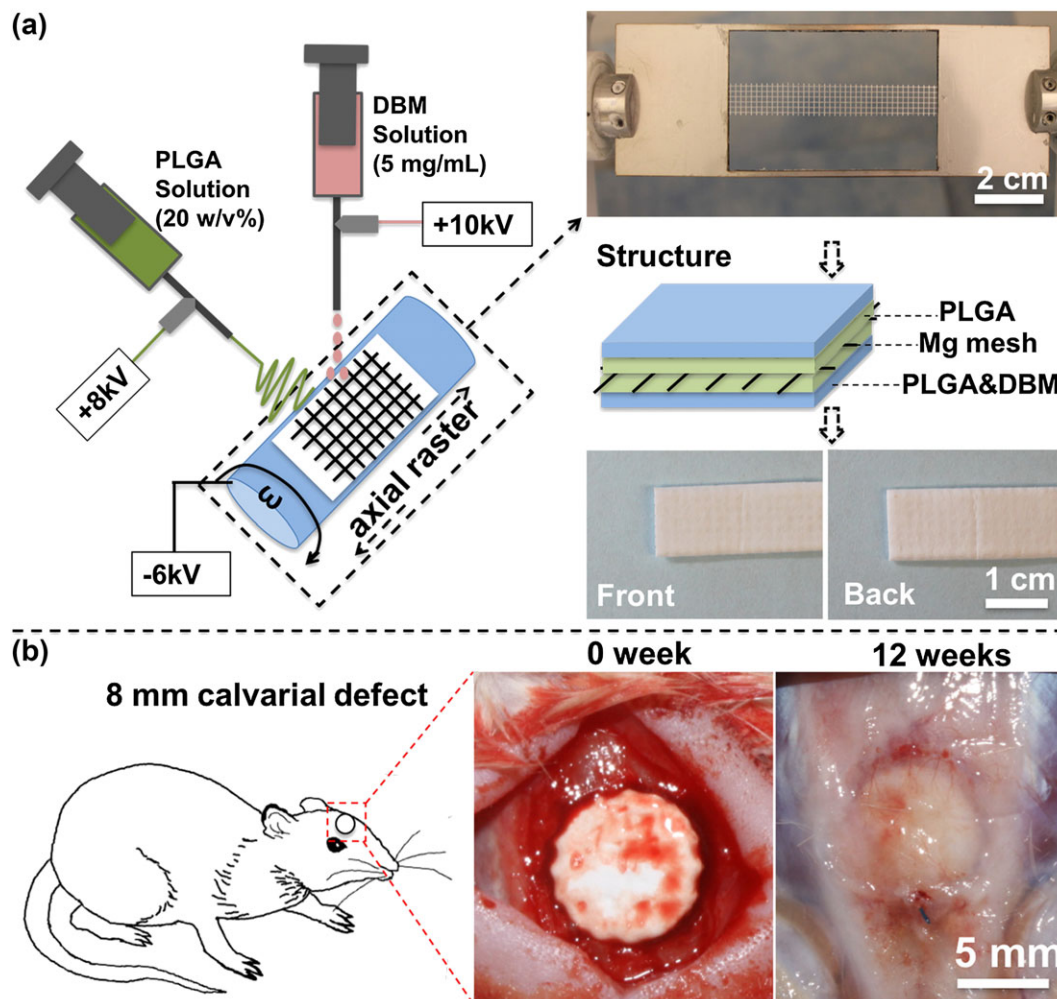


FIGURE 1 (a) Fabrication of Mg alloy mesh embedded with a poly(lactic-co-glycolic acid)/demineralized bone matrix (PLGA/DBM) composite scaffold and (b) schematic diagram of the scaffolds implanted into 8-mm calvarial defect for 12 weeks [Colour figure can be viewed at wileyonlinelibrary.com]

2 | EXPERIMENTAL

2.1 | Magnesium mesh fabrication

A rectangular sheet (200 × 500 mm, 250 μm thick) of AZ31 magnesium alloy was purchased from Goodfellow USA. According to the vendor, the alloy composition was 3% Al, 1% Zn, with the balance Mg. Using a methodology previously described (Shanov et al., 2017), photolithography was utilized to transfer a mesh pattern (with square-shaped pores of 1.5 × 1.5 mm) onto AZ31 foil, followed by chemical etching.

2.2 | Fabrication of Mg mesh reinforced PLGA/DBM hybrid scaffold

A concurrent electrospinning/electrospray method was used to fabricate the Mg alloy mesh reinforced PLGA/DBM hybrid composite scaffold (Figure 1a). Briefly, PLGA (85:15 LA : GA, MW~150,000 Da, PolySciTech, USA) in hexafluoroisopropanol (Sigma-Aldrich, USA) solution (20%, wt/vol) was fed at 1.5 ml/hr from a capillary perpendicularly located from a rotating stainless steel flat target. The target was

composed of two identical plates atop one another that each incorporated a cut out (60 × 40 mm). The Mg mesh (65 × 10 mm) was placed centrally in between the two plates to secure it in the centre of the open gap area (with 15 mm open gap on each side). The voltage of the target and PLGA solution capillary was -6 and + 8 kV, respectively. The distance between the central axis of target and the polymer infusing capillary was 170 mm. The target was rotated at 50 rpm while translating back and forth over a 6 cm distance along the rotational axis at 0.3 cm/s. After 2-hr deposition time, PLGA fibres encased the entire Mg mesh and the formerly open gap regions on each side of the mesh. At that time, the process was altered. DBM (Canine Demineralized Bone Matrix, Veterinary Transplant Services, Inc, USA) powder suspended at 5 mg/mL in sodium hyaluronate solution (HA700K-5, Lifecore Biomedical, USA, 2 mg/ml deionized (DI) water) at 4 °C was fed by a syringe pump into a capillary (1.2 mm I.D.) with an infusion rate of 2 ml/hr. The capillary was suspended above the rotating Mg mesh target and perpendicular to the capillary delivering the PLGA solution. The distance between the central axis of the target and the DBM infusing capillary was 70 mm. After 5 hr of concurrent electrospinning of PLGA and electro spraying of the DBM solution, the PLGA/DBM hybrid scaffold was obtained. The rectangular gap in

the two target plates was now composed of three sections. The central section was the Mg alloy mesh encased in the PLGA/DBM composite, whereas the flanking sections had deposited PLGA and PLGA/DBM but lacked the Mg alloy mesh. The three sections were separated by cutting lengthwise. After freeze-drying, the samples were stored at -20°C until further characterization.

2.3 | Hybrid scaffold characterization

Macroscopic images were taken by digital camera. The surface morphology and cross-sectional images of the Mg mesh encapsulated in PLGA/DBM were observed with scanning electron microscopy (SEM; JEOL 6330F) after gold sputtering. For cross-sectional preparation, the scaffold was frozen and broken in liquid nitrogen. Fluorescent images of the PLGA/DBM scaffold were taken for scaffolds where the polymer solution was labelled with fluorescein isothiocyanate, and the DBM particles were stained by rhodamine to clearly identify each component in the scaffold.

2.4 | Flexural strength measurement

Three-point bending tests were conducted to measure the flexural strength and flexural modulus of the hybrid scaffolds with and without Mg mesh. The measurements were performed in a bending test device (ElectroForce 3200 [Bose, MN]) according to a standard testing protocol. Specifically, the Mg mesh with PLGA/DBM scaffold ($15 \times 10 \times 1$ mm) or PLGA/DBM scaffold ($15 \times 10 \times 0.7$ mm) were placed on two supporting pins at a set distance of 12 mm and then bent under loading yield occurred. The flexural stress (σ_f ; Temenoff & Mikos, 2008) and flexural modulus (E_f ; Zweben, Smith, & Wardle, 1979) were obtained according to Equations (1) and (2):

$$\sigma_f = \frac{3FL}{2bd^2}, \quad (1)$$

$$E_f = \frac{L^3m}{4bd^3}, \quad (2)$$

where σ_f stands for the flexural stress (MPa); F is the load at a given point on the load deflection curve (N); L , b , and d represent support span (mm), width of test beam (mm), and depth or thickness of tested beam (mm), respectively; and m is related to the slope of the initial straight-line portion of the load deflection curve (N/mm).

2.5 | Rat bone mesenchymal stem cell culture study

Rat bone mesenchymal stem cells (BMSCs; OriCell Fisher 344 [F344], Cyagen, USA) were cultured in OriCell MSC Growth Medium (Cyagen) in a humidified incubator under 5% CO_2 at $37 \pm 0.5^{\circ}\text{C}$. Then, the BMSCs (under an original passage number of 10) were digested by trypsin, and the cells were seeded on the scaffold (10 mm diameter, punched from the original scaffolds) at a density of 2×10^4 cells/ml. After 3-hr incubation to allow cell attachment, the samples were transferred into a new 24-well plate for further culture. Tissue culture polystyrene discs of the same size as the samples were similarly

seeded with cells and cultured with OriCell MSC Growth Medium or Osteogenic Differentiation Basal Medium (GUXMX-03021-175, Cyagen, USA), respectively, to serve as negative and positive controls. The proliferation of BMSCs on the scaffolds was assessed using an MTS assay kit (Promega CellTiter 96 Cell Proliferation Assay, $n = 4$). After 1-, 3-, and 7-day culture, the samples were carefully transferred into a new 24-well plate, and then, 0.5-ml cell culture medium mixed with MTS reagent (9:1) was added. After 3-hr incubation, 150 μl of the medium was carefully transferred to a 96-well. The optical density was measured at 490 nm using a microplate reader. For SEM observations of cells adhered on the scaffolds, after 7-day culture, the scaffolds were washed with pre-warmed phosphate-buffered saline (PBS) three times. Then, the cells on the scaffolds were fixed with 2.5% glutaraldehyde. After that, the cells were subjected to dehydration in graded series of alcohol/DI water solutions (30%, 50%, 70%, 90%, and 100%) for 15 min each. The samples were then immersed in hexamethyldisilazane for 5 min. Finally, the scaffolds with cells were gold-sputtered prior to SEM observation.

Alkaline phosphatase (ALP), as an early osteogenic differentiation marker (Yao et al., 2017), is a hydrolase enzyme responsible for removing phosphate groups from many types of molecules. After 7- and 14-day culture, the samples were washed with PBS three times, and the cells on the sample surface were lysed with 0.2 ml 1% (vol/vol) Triton X-100 for 12 hr at 4°C . Then, the cell lysate solution was centrifuged, and the supernatant was used for ALP activity assessment. The total protein concentration of the cell lysate for each sample was measured using the bicinchoninic acid (Sigma-Aldrich, USA) protein assay kit. The final ALP activity was normalized with respect to the total protein content obtained from the same cell lysate. The number of independent samples used for statistics was no less than four, and all of the assays were repeated more than two times.

For calcium deposition assessment, after 21 days of BMSC culture, the samples were carefully transferred into a new 24-well plate and washed with pre-warmed PBS three times. Alizarin red solution (1 ml of 2%; Sigma-Aldrich, USA) was slowly added to each well and then incubated for 20 min at room temperature. After that, the excess dye was removed from each well and washed several times with DI water until no further removal was observed, as verified by comparison of optical densities using a microplate reader of the DI water used as a wash with pristine DI water. Samples were then imaged macroscopically. For quantification of alizarin red staining, the samples were treated with 150 μl 10 wt% hexadecylpyridinium chloride (Sigma-Aldrich, USA)/PBS solution to solubilize the dye, followed by measurement of absorbance at 570 nm with a microplate reader (Zhu, Mao, & Gao, 2013).

2.6 | In vivo animal study and surgical procedures

Female Sprague–Dawley rats (150–170 g) were purchased from Harlan Sprague Dawley Inc., USA. All animal procedures were performed as approved by the Institutional Animal Care and Use Committee of the University of Pittsburgh. The surgical procedure was similar to that reported in reference (Spicer et al., 2012). The rats were randomly divided into five groups ($n = 5$ each group). After anaesthetization with 10% chloral hydrate (4 ml/kg), the rats were shaved on the head, and

the epicranium was cut longitudinally. The critical-sized calvarial defect (8 mm diameter) was made using a dental drill. The scaffold samples were cut in a disc (8 mm diameter) using a punch. The disc samples were then physically placed in the defect, and the wound was carefully sutured. After 12-week implantation, the rats were anaesthetized with 10% chloral hydrate (4 mL/kg), and 3D computed tomography data of the rat calvaria were obtained with a Vivo 40 micro-CT system (Scanco, Switzerland).

2.7 | Histological assessment and immunohistochemical staining

After a 12-week implant period, the rats were anaesthetized and sacrificed. The whole calvaria was removed and fixed in 4% paraformaldehyde solution for 1 week. The harvested calvaria were dehydrated with an increasing series of ethanol baths (70%, 75%, 80%, 85%, 90%, 95%, and 100%) for 24 hr each and were then embedded in paraffin. The cross section of the central area of the defects were cut (5 μ m thick) for further histological evaluation. Haematoxylin and eosin (H&E) and Masson's trichrome staining were performed on isolated sections, as was Von Kossa staining to confirm the presence of calcified tissue (Von Kossa kit, Abcam, USA).

Immunohistochemical staining of osteocalcin (OCN) was investigated to examine osteogenesis. Sections of explanted tissue were deparaffinized by dipping in xylene three times (3 min for each), followed by 100%, 95%, and 70% ethanol washes for 1 min each and running water for 2 min, respectively. Subsequently, the sections were immersed in an antigen retrieval buffer (HistoVT One, Nacalai Tesque, INC. Japan) at 95–100 °C for 20 min to expose the antigen on the surface. After the buffer solution was cooled to room temperature, the sections were washed with PBS three times (3 min for each) and then incubated in blocking solution (2% normal horse serum, 1% BSA, 0.1% Triton X-100, and 0.1% Tween-20 in 1 \times PBS, pH 7.4) in a humidified chamber for 1 hr at room temperature to inhibit non-specific binding. After removing the blocking solution, the primary antibody of OCN (Osteocalcin antibody, orb259644, Biobyte, USA) diluted in blocking solution (2.5 μ g/ml [1:200]) was added to cover the sections and incubated in a humidified chamber at 4 °C overnight. After removing the primary antibody, the slices were washed with PBS three times (3 min for each). The fluorescently labelled secondary antibody (donkey anti-rabbit, ab150073, Abcam, USA) diluted in blocking solution (1:450) was added to the sections and incubated in a humidified chamber at room temperature in the dark for 1 hr. After removing the secondary antibody, the slices were washed with PBS three times (3 min for each). Finally, nuclei were stained with 4',6-diamidino-2-phenylindole (DAPI; 1:10000, Sigma, USA). For each sample, more than five different microscopic images were taken under fluorescence microscopy to view OCN-positive structures.

2.8 | Statistical analyses

All the data are expressed as mean \pm standard deviation (as error bars in figures) determined from at least four independent experiments. The statistical analyses performed to evaluate differences were one-way

analysis of variance, with post hoc Newman–Keuls testing, where a *p* value of less than .05 was considered to be statistically significant.

3 | RESULTS

3.1 | Morphology and mechanics of Mg mesh reinforced PLGA/DBM hybrid scaffold

Figure 2a–d shows the formed composite material of the Mg mesh integrated within the polymer/ECM (PLGA/DBM) hybrid material from a macroscopic and microscopic perspective. The surface of deposited PLGA fibres had a fibre diameter of 3 ± 0.5 μ m, and scaffold cross sections showed encapsulation of the Mg mesh by polymer fibres. In Figure 2d, distinct regions of DBM (green, labelled with fluorescein isothiocyanate) could be seen to be distributed among the red PLGA fibres.

The flexural strength and modulus of the PLGA/DBM hybrid scaffolds with and without Mg mesh as examined by three-point bending are seen in Figure 2e,f. As expected, the Mg mesh strengthened and stiffened the polymer/ECM hybrid scaffold.

3.2 | In vitro ALP activity and calcium deposition

Figure 3a demonstrates increasing ALP activity with culture time for BMSCs cultured on the various scaffolds. The ALP activity on PLGA/DBM hybrid scaffold (PLGA@HA&DBM) was higher than that for the scaffold without DBM (PLGA@HA), and this activity was further increased when the Mg mesh was included (Mg-PLGA@HA&DBM) at 7 and 14 days of culture.

Alizarin red staining is shown qualitatively and quantitatively in Figure 3b,c for BMSCs cultured on scaffolds for 21 days. Measurements of optical density of the dissolved alizarin red that had bound to the cultured surfaces were greater for PLGA@HA&DBM and Mg-PLGA@HA&DBM, consistent with greater calcium deposition. Furthermore, Mg-PLGA@HA&DBM had greater alizarin red binding than PLGA@HA&DBM, indicating an effect attributable to the presence of the Mg mesh. The qualitative images were consistent with these findings.

3.3 | In vivo animal study

3.3.1 | Masson trichrome staining and H&E staining

The in vivo osteogenic properties of the scaffolds were investigated in a critical-sized calvarial defect for 12 weeks as represented in Figure 1 b. In Figure 4a,b, representative Masson trichrome-stained sections are presented together with quantitative image analysis of all stained areas and blue-stained areas (black arrow) measured from trichrome-stained sections from scaffolds after 12-week implantation. The staining patterns in Mg-PLGA@HA&DBM and PLGA@HA&DBM showed more general staining as well as more blue-stained areas compared with the other scaffold types. Also, the Mg-PLGA@HA&DBM displayed more blue-stained areas compared with PLGA@HA&DBM. There was also more general and blue staining observed on Mg-PLGA@HA scaffolds than PLGA@HA scaffolds. Blue staining was obvious and consistently present in the regions surrounding what

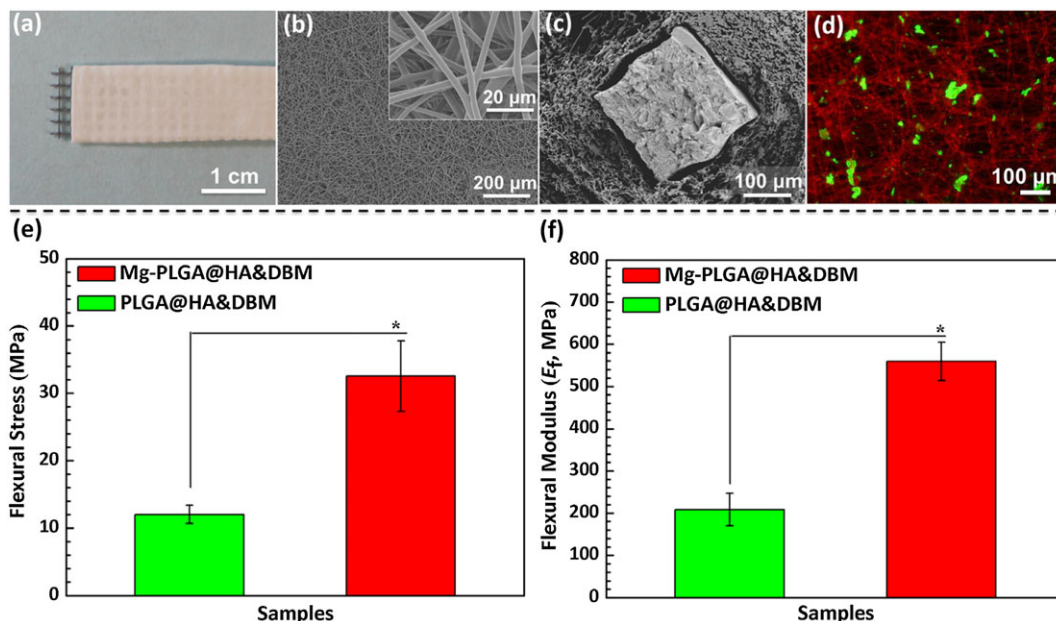


FIGURE 2 Hybrid scaffold characterization of Mg mesh reinforced poly(lactic-co-glycolic acid)/demineralized bone matrix (PLGA/DBM) scaffold: (a) macroscopic images of fabricated scaffold, (b) scanning electron microscopy image of PLGA electrospun fibers, (c) cross-sectional morphology of the scaffold, and (d) fluorescent image of the Mg mesh reinforced PLGA/DBM scaffold, polymer solution labelled with fluorescein isothiocyanate, and DBM particles stained by the rhodamine for identifying polymer fibre and DBM in the scaffolds, and (e) flexural stress and (f) flexural modulus of PLGA/DBM hybrid scaffold with and without Mg mesh ($p < .05$) [Colour figure can be viewed at wileyonlinelibrary.com]

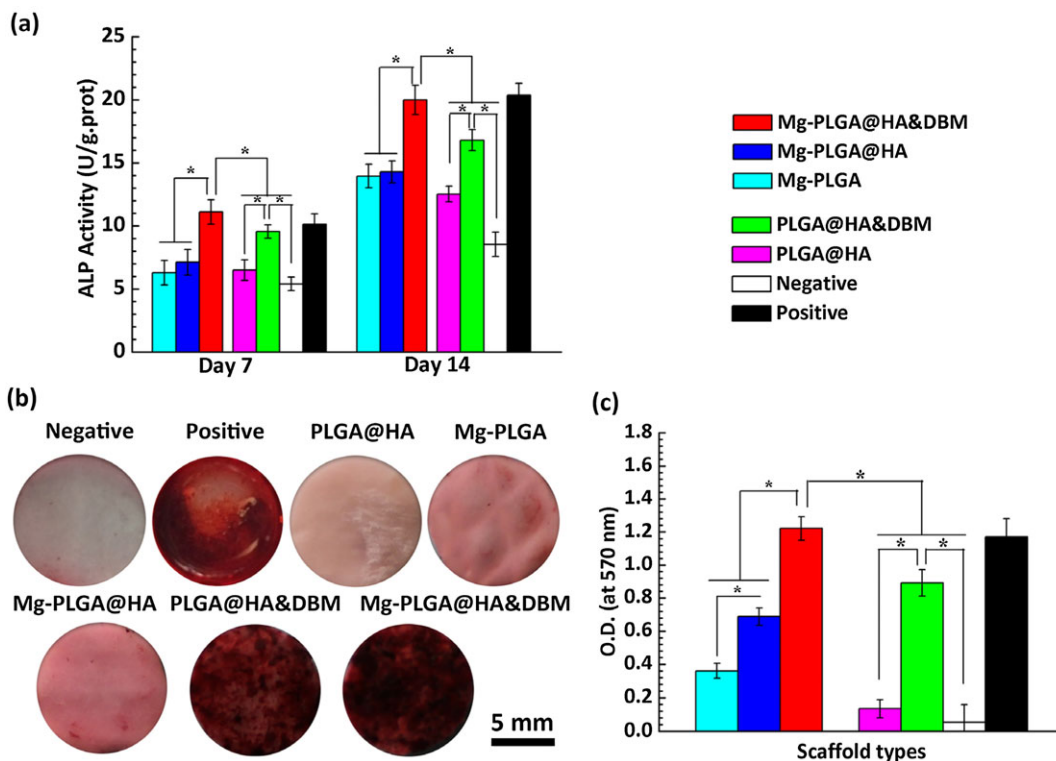


FIGURE 3 (a) Alkaline phosphatase (ALP) activity results of the scaffolds after 7 and 14 days of bone marrow stem cell (BMSC) culture ($p < .05$) and (b) alizarin red staining and (c) alizarin red quantity after BMSC seeded on scaffolds for 21 days ($p < .05$). DBM = demineralized bone matrix; HA = hyaluronic acid; PLGA = poly(lactic-co-glycolic acid) [Colour figure can be viewed at wileyonlinelibrary.com]

appeared to be voids left behind by the Mg struts (red arrows). The negative control group, where no implant was made, presented a very thin tissue covering over the defect.

H&E staining and analysis of recovered tissue sections from the defect site are presented in Figure 4c. Consistent with the Masson trichrome staining results, more staining was present on Mg-

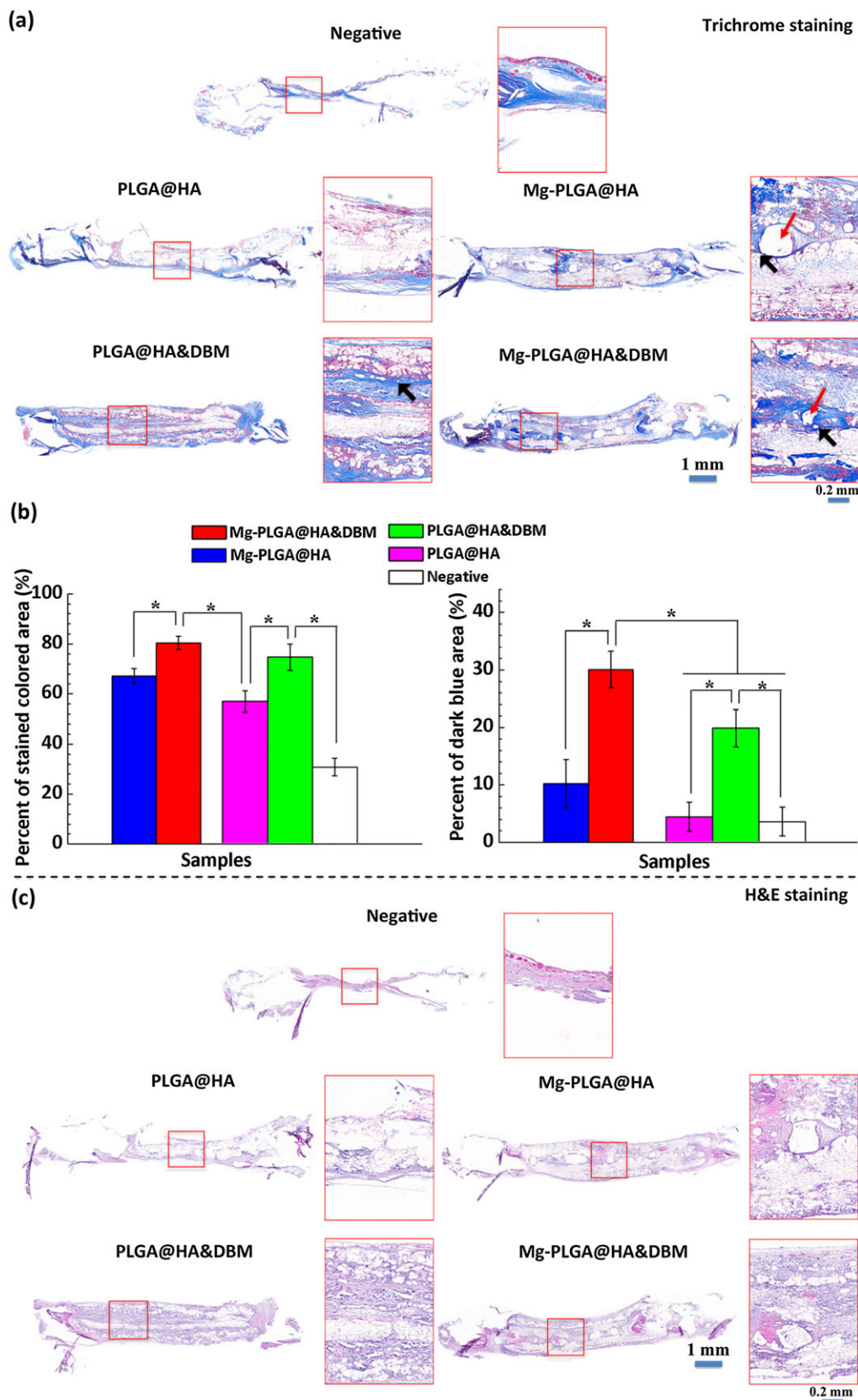


FIGURE 4 (a) Masson trichrome staining of scaffolds after implantation for 12 weeks, (b) the quantification for stained coloured area (assumed as tissue ingrowth area, left) and dark blue area (black arrow, assumed as mineralized tissue, right) of Mg-PLGA@HA&DBM, PLGA@HA&DBM, Mg-PLGA@HA, PLGA@HA, and Negative groups after 12 weeks of implantation in critical-sized calvarial defect ($n = 5$, * $p < .05$), and (c) haematoxylin and eosin (H&E) staining of Mg-PLGA@HA&DBM, PLGA@HA&DBM, Mg-PLGA@HA, PLGA@HA scaffolds, and Negative control after implanted for 12 weeks. Deep pink-coloured area (black arrow) was noticeable around Mg struts (red arrow) for the Mg-PLGA@HA&DBM. DBM = demineralized bone matrix; HA = hyaluronic acid; PLGA = poly(lactic-co-glycolic acid) [Colour figure can be viewed at wileyonlinelibrary.com]

PLGA@HA&DBM and PLGA@HA&DBM scaffolds compared with the others, and Mg-PLGA@HA scaffold displayed more stained area than that of the PLGA@HA scaffold. The negative control revealed minimal staining. As shown in magnified images, Mg-PLGA@HA&DBM and Mg-PLGA@HA scaffolds presented some regions (black arrows) noticeable around Mg struts (red arrow) that had a staining and morphology consistent with new forming bone.

3.3.2 | Von Kossa staining

With Von Kossa staining (Figure 5), regions stained black that would be consistent with phosphate deposits, including calcium phosphate and magnesium phosphate, were quantified. No such staining was found in the negative control sections, with staining only present in the peripheral bony regions of the defect. PLGA@HA displayed very sparse stained areas that increased modestly with the presence of the Mg mesh. A noticeable increase in staining was present with the PLGA@HA&DBM scaffold versus the Mg-PLGA@HA, despite the lack of Mg, whereas the strongest staining was when both

DBM and Mg were present in the Mg-PLGA@HA&DBM. The quantitative results in Figure 5b confirmed these observations.

3.3.3 | Immunohistochemical staining

Immunohistochemical staining was examined to further assess OCN expression in the implanted scaffolds after 12 weeks. Immunohistochemical OCN staining and quantification of positively labelled cell number and area of labelling are shown in Figure 6. The quantitative results showed that Mg-PLGA@HA&DBM scaffold presented both a larger number of positively stained cells and a greater area of OCN-positive staining than all of the other scaffold types and the negative control. Both the addition of Mg and the addition of DBM increased the OCN-stained area versus the scaffolds lacking these components.

4 | DISCUSSION

The biomaterials community interest in magnesium-based alloys for bone applications has grown dramatically in recent years. Mg-based

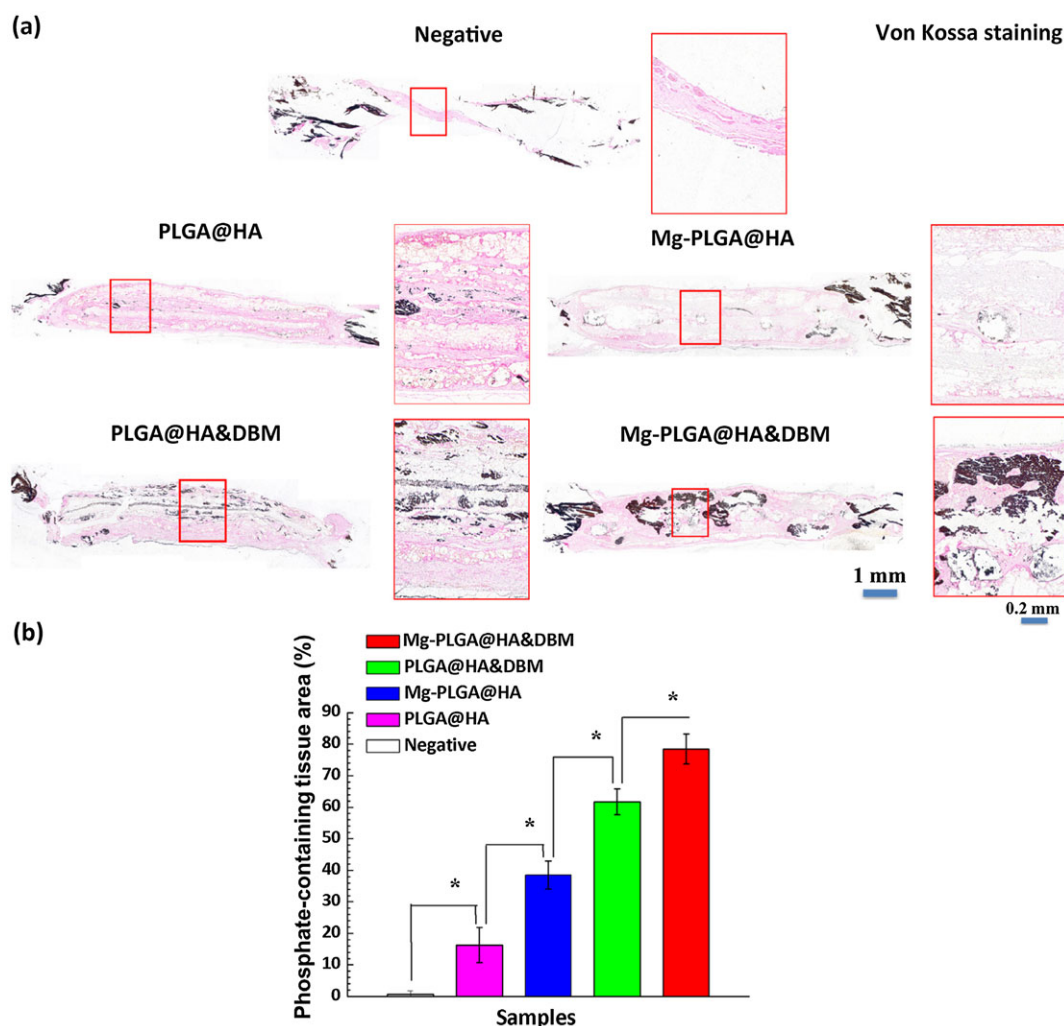


FIGURE 5 (a) Von Kossa staining of scaffolds after implantation in critical-sized calvarial defects for 12 weeks. The black and pink areas represent the phosphate-containing tissues (calcium phosphate and magnesium phosphate) and cytoplasm in the regenerated bone tissue, respectively. (b) The quantification for calcified bone-like area of Mg-PLGA@HA&DBM, PLGA@HA&DBM, Mg-PLGA@HA, PLGA@HA, and Negative groups after 12-week implantation ($n = 5$, $*p < .05$). DBM = demineralized bone matrix; HA = hyaluronic acid; PLGA = poly(lactic-co-glycolic acid) [Colour figure can be viewed at wileyonlinelibrary.com]

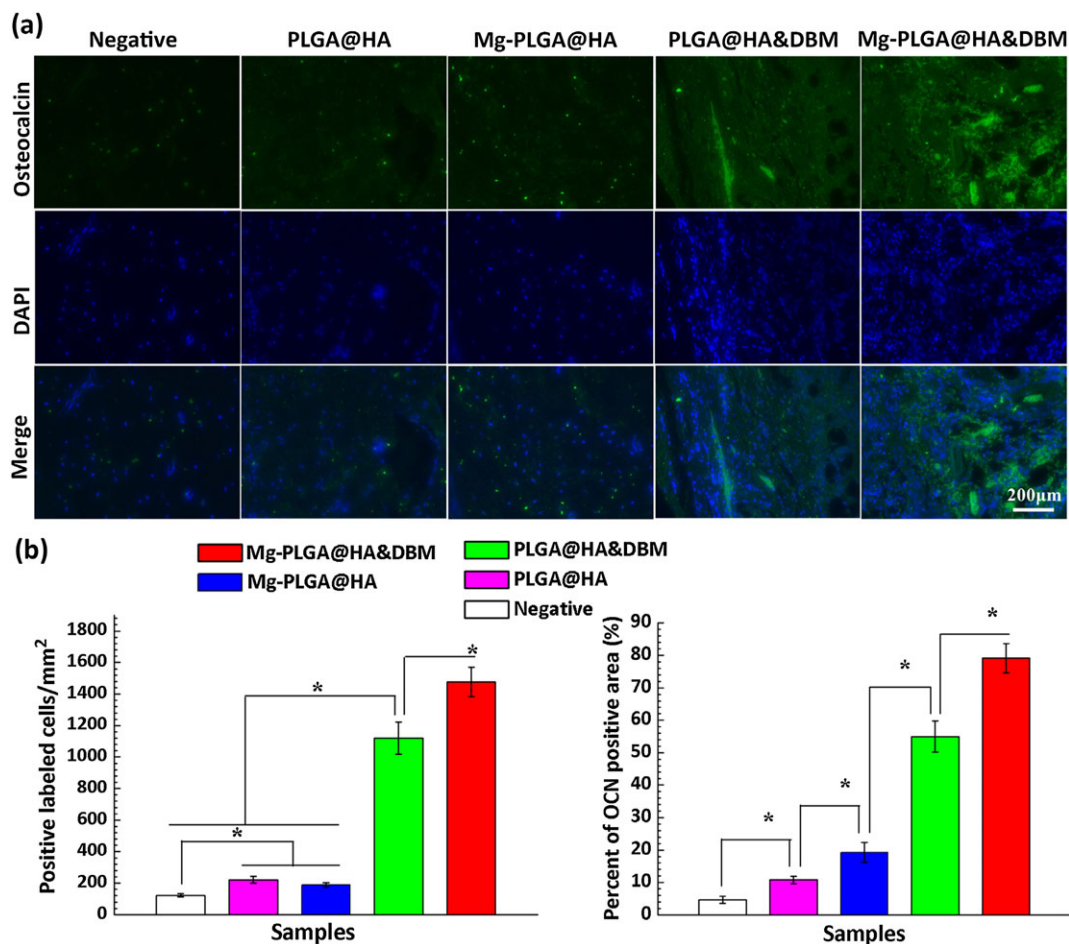


FIGURE 6 (a) Immunohistochemical staining of the osteogenic marker (Osteocalcin [OCN]) of scaffolds after implantation in a critical-sized calvarial defect for 12 weeks. Blue and green areas represent cell nuclei and OCN expression, respectively. (b) The quantification for bone-related cell numbers and OCN protein expression area of Mg-PLGA@HA&DBM, PLGA@HA&DBM, Mg-PLGA@HA, and PLGA@HA implanted in critical-sized calvarial defect for 12 weeks as compared with Negative control ($n = 5$, $^*p < .05$). DBM = demineralized bone matrix; HA = hyaluronic acid; PLGA = poly(lactic-co-glycolic acid) [Colour figure can be viewed at wileyonlinelibrary.com]

materials or additives, such as Mg screws (Han et al., 2015), plates (Chaya, Yoshizawa, Verdalis, Noorani, et al., 2015; Chaya, Yoshizawa, Verdalis, Myers, et al., 2015), wires (Li et al., 2017; Li, Chu, et al., 2015; Li, Wang, et al., 2015; Li, Zhou, et al., 2015), fibres (Wu, Ibrahim, et al., 2013; Wu, Li, et al., 2013), particles (Ma et al., 2015; Shi, Pei, et al., 2017; Shi, Wang, et al., 2017), and Mg ions (Chen et al., 2014; Mouri o, Cattalini, & Boccaccini, 2012) have been utilized as, or incorporated into, bone scaffolds or coatings to positive effect in terms of mechanical properties, osteogenesis, and healing outcomes (Ma et al., 2015). The Mg alloy mesh utilized in the reported composite scaffold provided critical mechanical properties and served to improve the *in vitro* osteogenic activity. The open mesh structure facilitated integration of the polymer and DBM with the structural elements and later provided for tissue integration around the Mg alloy elements. As expected, the flexural stress and modulus of the PLGA@HA&DBM scaffold were significantly increased with inclusion of the mesh. Both DBM and the Mg mesh present *in vitro* osteopromotive effect (Figure 3) and *in vivo* bone regeneration were also improved. Though no specific, isolated biological agents inducing osteogenic differentiation, such as plasmid DNA, PDGF, or BMP-2, were added in this study, DBM has been shown to retain some BMP proteins and collagens (Wildemann, Kadow-Romacker, Haas, & Schmidmaier, 2010). For prior

studies in the rat model with DBM inclusion (Ding et al., 2015; Dozza et al., 2017), correlations between osteogenic gene expression and ALP/calcium deposition have shown, specifically that DBM was associated with osteogenic gene expression, including COL1A1, ALP, OCN, and ONN. The effect of adding Mg to the polymer/DBM scaffold is consistent with earlier reports with Mg-containing materials (Liu et al., 2016). The BMSC proliferative ability also appeared to be stronger with both DBM and Mg present, as evidenced by qualitative SEM images of cells on the scaffolds. Supporting this finding were results from an MTT metabolic activity assay (Figure S1). However, it is known that the corrosion of Mg affects MTT results (Fischer et al., 2010), so the MTT data alone do not provide adequate evidence of the phenomenon. In observing the histological images from the rat implants, it is notable how new bone appeared to be regenerating preferentially in the vicinity of the Mg mesh struts. This was seen in the trichrome (Figure 4a,b), H&E (Figure 4c), and von Kossa staining (Figure 5). Further confirmation of this effect was found in the micro-computed tomography images (Figure S2) where solid areas were visible along the Mg struts in Mg-PLGA@HA and Mg-PLGA@HA&DBM scaffolds, providing an outline of the originally implanted Mg mesh. This may be attributed to the Mg ions released by corrosion of magnesium promoting *in vivo* osteogenesis, consistent

with published reports (Chaya, Yoshizawa, Verdelis, Noorani, et al., 2015; Chaya, Yoshizawa, Verdelis, Myers, et al., 2015). The majority of reported magnesium containing scaffolds for repair of calvarial bone defects have been concentrated on magnesium phosphate ceramics (Kim et al., 2016) and magnesium-doped scaffolds (Deng, Li, Yang, Xie, & Kang, 2017; Sun et al., 2016). In contrast, the authors are not aware of reports of metallic Mg-based alloy incorporated in a bone scaffold for calvarial bone defect repair. This study has attempted to fill this gap by incorporating metallic magnesium as a key component in a composite designed to facilitate critical-sized calvarial defect healing.

Currently, a variety of biodegradable polymeric scaffolds, having different porous morphologies created using different methods, have been employed to repair critical-sized calvarial bone defects. The most commonly utilized biodegradable polymers include PLGA (Gentile, Chiono, Carmagnola, & Hatton, 2014), poly(L-lactic acid) (Huang et al., 2017), poly(ϵ -caprolactone) (Wongsupa, Nuntanarant, Kamolmattayakul, & Thuaksuban, 2017), and copolymers with these common polyesters (Wang et al., 2016). One of the effective strategies to improve the *in vitro* and *in vivo* osteogenesis of polymeric scaffolds has been the incorporation of bioactive reagents for controlled delivery to the defect region (Yassin et al., 2017). Most commonly, bone morphogenetic proteins (BMPs, and BMP-2 in particular; Fan et al., 2015; Huang et al., 2017) and peptide derivatives (Lee et al., 2017) have shown effective bone regeneration in many studies, and this concept has translated to clinical utilization in some settings (Govender et al., 2002; Valentin-Opran, Wozney, Csimma, Lilly, & Riedel, 2002). However, recent studies have highlighted morbidities associated with the release of BMP-2 in some clinical applications that include post-operative inflammation, ectopic bone formation, osteolysis and subsidence, and others (James et al., 2016). Relatively high concentrations of BMP-2 in the scaffold may be an issue for the placement of such devices in some locations and in some patient populations. Although further experience and design refinement may help to address these issues, it would be attractive to have an alternative approach that did not rely upon such an exogenous growth factor from both a safety and economic perspective.

To date, no suitable alternative has been broadly reported to have such effective bone regenerative efficacy as BMP-2. In considering alternatives that do not rely upon the controlled release of a purified growth factor, DBM presents a bioactive alternative. This bone-derived product provides an array of biologically active molecules, including BMP-2 and a variety of other growth factors at more physiologic concentrations (Wildemann et al., 2010), as well as collagens and other ECM components to promote osteoconduction and osteoinduction (Khoshzaban et al., 2011). Although DBM has been shown to be effective in some preclinical bone healing scenarios (Alidadi, Oryan, Bigham-Sadegh, & Moshiri, 2017; Dozza et al., 2017), there is less evidence of efficacy in clinical trials (Kinney, Ziran, Hirshorn, Schlatterer, & Ganey, 2010), and in several preclinical studies, the osteogenic efficacy of DBM alone may not be enough (Rhee et al., 2011; Van Houdt et al., 2017). Further, the material presents some challenges associated with handling, stability after surgery, and identification of an appropriate carrier (Maddox, Zhan, Mundy, Drohan, & Burgess, 2004). A common difficulty in comparing DBM

evaluation studies is the variability introduced based on the source of DBM and the effect of donor and processing methodology on the level of retained bioactivity (Bae et al., 2006). In this report, a commercial canine source of DBM was utilized, which had been shown to have efficacy in the canine model (Hoffer, Griffon, Schaeffer, Johnson, & Thomas, 2008). Although the use of xenogenic material in the rat model may have reduced activity compared with an allogenic source (Wang & Glimcher, 1999), other reports have shown the use of xenogenic DBM to positive effect (Bigham, Dehghani, Shafiei, & Nezhad, 2008).

DBM has been frequently evaluated for the repair of rat calvarial defects (Acarturk & Hollinger, 2006; Rhee et al., 2011; Townsend et al., 2017). Generalizing across studies, DBM was associated with a positive effect, but the efficacy of DBM alone was limited. Comparing literature reports of DBM-alone cases (Rhee et al., 2011; Stancoven et al., 2013), the PLGA@HA&DBM scaffold in this study appeared to have a better bone regenerative efficacy in the rat critical-sized calvarial defect. This may be attributable to the porous structure of this scaffold, the osteogenic efficacy of canine DBM, or possibly the DBM loading strategy that benefit to the release of bioactive agents. Commonly used strategies to improve the osteogenic efficacy of DBM have been to incorporate additional bioactive reagents, which include BMP-2 (Townsend et al., 2017), the stromal vascular fraction cells (Rhee et al., 2011), and others. Comparing with DBM that has been combined with BMP-2 (Townsend et al., 2017), Mg alloy mesh reinforced PLGA/DBM scaffold in this study had a lower osteogenic efficacy, which can be attributed to the recognized osteogenic efficacy of BMP-2. In addition, DBM combined with polymer in some cases has a slower bone regeneration rate compared with DBM alone (Rhee et al., 2011), which may be due to the acidic degradation products of the polymer component aggravating local inflammatory reactions.

In this study, PLGA was utilized as a secondary structural component and was selected for its common application in a variety of approved medical devices. The PLGA provided a three-dimensional porous structure that could facilitate nutrient transfer, as well as provide a reservoir to hold the DBM and hyaluronic acid (HA) mixture. The *in vivo* results showed that bone regenerative efficacy of Mg alloy mesh reinforced PLGA/DBM scaffold was not at the level achievable by BMP-supplemented matrices. One would expect BMP provision to improve the results, but as noted above, there is interest in developing scaffolding materials that avoid such exogenous factor incorporation. However, other factors may have limited the bone regeneration response, including the slower degradation rate of higher molecular weight PLGA that may have occupied space, discouraging bone tissue ingrowth. The combination of PLGA and Mg alloy mesh might be expected to moderate the side effects from acidic degradation products of PLGA because of the alkaline corrosion products of Mg as measured in previous publications (Wen, Zou, Luo, & Zhou, 2017; Wu, Ibrahim, et al., 2013; Wu, Li, et al., 2013; Xu, Kim, Stahl, & Nukavarapu, 2018). It is not clear how the PLGA and Mg mesh components will specifically interact with each other to accelerate or slow the degradation of each material *in vivo*. The acidic environment generated from the PLGA degradation could accelerate both corrosion of Mg and degradation of PLGA; however, the mild alkaline surroundings of the Mg alloy degradation might slow these degradation processes.

The concurrent electrospinning and electrospray method used in this study resulted in the porous structure of this scaffold (in Figure 2) and facile loading and delivery of DBM. The rotating target holding the Mg mesh ensured the Mg mesh was encapsulated by the PLGA fibres (as shown in Figure 2c) as well as DBM particles being distributed into the scaffold. It has been shown that the loading strategy of DBM into composite materials can have a large effect on the delivery and release of its bioactive components and thus the resulting bone regenerative efficacy (Ding et al., 2015). In this study, viscous hyaluronic acid (HA) was used to suspend DBM particles, which made the electrospraying process easier to accomplish. HA has previously been reported as an effective DBM carrier (Gruskin et al., 2012). The concentration of HA to suspend DBM particles was optimized to a range where higher or lower concentrations would not be suitable for electrospraying or DBM particle suspension.

Several limitations of this study are worth specifically noting and considering. First, as can be seen from the *in vivo* results, complete defect filling with regenerated calcified tissue was not achieved. Other reports using similar models have demonstrated complete or near complete defect filling. However, as noted above, most of these reports have relied upon controlled growth factor release (e.g., BMP-2; Li, Chu, et al., 2015; Li, Wang, et al., 2015; Li, Zhou, et al., 2015; Lee et al., 2017; Wang, Wang, et al., 2015; Wang, Witte, et al., 2015). Because the incorporation and release of exogenous growth factors have been associated with complications in some application areas (Epstein, 2013; James et al., 2016) and add substantial cost to a product, the avoidance of such a design feature has merit. Furthermore, an 8-mm-diameter defect size was chosen as a critical-sized calvarial defect, which is considered as one of the most aggressive sizes for a rat (Spicer et al., 2012). Because our primary target design was a mechanically reinforced hybrid scaffold with the biodegradable Mg mesh, it was considered that the mechanically strengthened scaffold might have further potential to heal larger sized defects requiring such mechanical support at the initial stage, as well as receiving potential osteopromotive activity from the released Mg ions. Another limitation of the study is that only one time point was evaluated in this study, and a later point may have yielded further calcified tissue elaboration, although a faster healing response would be desirable clinically. The calvarial defect regenerative degree experienced with the scaffolds after 4- and 8-week implantation periods was observed using nondestructive micro-computed tomography testing; however, no extensive bone regeneration was observed at those time points. Further long-term implantation studies may be required to optimize the hybrid scaffold composition. It is notable that some of the polymer appeared macroscopically and in tissue sections to remain at the defect site. Because the polymer was not of primary importance structurally and principally served as a space filler and to carry the DBM, a faster degrading polymer system would be of interest to facilitate earlier tissue ingrowth. Finally, the described system might be optimized by altering the Mg alloy/polymer/DBM ratio. In this report, the ratio of components was not varied. The ratio of components utilized was selected to fabricate a homogenous hybrid scaffold with similar thickness to rat calvarial bone. There were some processing-related design constraints related to material availability (i.e., Mg mesh thickness) and electroprocessing to achieve a fluid

capable of electrospraying. However, alternatives would be possible. For instance, a Mg mesh with denser, thinner wires might be desirable as might a greater level of DBM incorporation.

5 | CONCLUSIONS

A Mg mesh reinforced polymer/ECM (PLGA/DBM) hybrid scaffold was successfully fabricated by a concurrent method of electrospinning of PLGA solution and electrospray of DBM suspending in HA solution. The hybrid scaffold characterization results revealed that (a) Mg alloy mesh was encapsulated by PLGA fibres, and (b) DBM particles were distributed in this scaffold. As one would expect, the flexural stress and modulus of PLGA/DBM hybrid scaffold were significantly improved by the reinforced Mg alloy mesh. The Mg mesh reinforced PLGA/DBM hybrid scaffold promoted *in vitro* osteogenic differentiation of BMSCs as well stimulated bone regeneration in rat calvarial defects as compared with the other control scaffolds. The combination of DBM and Mg alloy mesh in this hybrid scaffold showed a combined beneficial effect *in vitro* and in a critical-sized bone defect model. Taken together, these results suggest that this Mg alloy mesh reinforced polymer/ECM hybrid scaffold has potential in the critical-sized bone regeneration where supplementation with exogenous growth factor is not employed.

ACKNOWLEDGEMENTS

This work was financially supported by the U.S. National Science Foundation (ERC-RMB, Award NSF 0812348), National Natural Science Foundation of China (21473138), National Key R&D Program of China (2016YFC1102500), Sichuan Youth Science & Technology Foundation (2012JQ0001), Education Program for Innovation & Entrepreneurship for Southwest Jiaotong University, and China Scholarship Council 201507000009.

CONFLICT OF INTEREST

The authors declared no conflicts of interest.

AUTHORS CONTRIBUTIONS

Dr. Yingqi Chen designed the study, pushed the idea to practice, collected and summarized the data, and wrote the manuscript. Dr. Sang-Ho Ye provided segmental data and partially helped with the data analysis, data summary, and manuscript draft. Mr. Hideyoshi Sato, a medical doctor, conducted the animal study and helped with the animal study experiment part draft. Dr. Yang Zhu helped with the part of data collection. Dr. Vesselin Shanov and Mr. Tarannum Tiasha provided the expected Mg mesh, which was designed by Dr. Yingqi Chen. Dr. Antonio D'Amore and Mr. Samuel Luketich helped with the mechanical property tests. Dr. & Prof. Guojiang Wan and Dr. & Prof. William R. Wagner are mentors of Dr. Yingqi Chen. Dr. & Prof. Guojiang Wan helped with the study design and provided insightful comments when the manuscript was being prepared. Dr. & Prof. William R. Wagner proposed this idea, supported and supervised this project, and provided intelligence and revised the manuscript.

ORCID

Yingqi Chen  <http://orcid.org/0000-0003-0982-1385>

REFERENCES

- Acarturk, T. O., & Hollinger, J. O. (2006). Commercially available demineralized bone matrix compositions to regenerate calvarial critical-sized bone defects. *Plastic and Reconstructive Surgery*, *118*, 862–873. <https://doi.org/10.1097/01.prs.0000232385.81219.87>
- Agarwal, S., Curtin, J., Duffy, B., & Jaiswal, S. (2016). Biodegradable magnesium alloys for orthopaedic applications: A review on corrosion, biocompatibility and surface modifications. *Materials Science and Engineering: C*, *68*, 948–963. <https://doi.org/10.1016/j.msec.2016.06.020>
- Alidadi, S., Oryan, A., Bigham-Sadegh, A., & Moshiri, A. (2017). Comparative study on the healing potential of chitosan, polymethylmethacrylate, and demineralized bone matrix in radial bone defects of rat. *Carbohydrate Polymers*, *166*, 236–248. <https://doi.org/10.1016/j.carbpol.2017.02.087>
- Amini, A. R., Laurencin, C. T., & Nukavarapu, S. P. (2012). Bone tissue engineering: Recent advances and challenges. *Critical Reviews in Biomedical Engineering*, *40*, 363–408. <https://doi.org/10.1615/CritRevBiomedEng.v40.i5.10>
- Bae, H. W., Zhao, L., Kanim, L. E., Wong, P., Delamarter, R. B., & Dawson, E. G. (2006). Intervariability and intravariability of bone morphogenetic proteins in commercially available demineralized bone matrix products. *Spine*, *31*, 1299–1306. <https://doi.org/10.1097/01.brs.0000218581.92992.b7>
- Bigham, A. S., Dehghani, S. N., Shafiei, Z., & Nezhad, S. T. (2008). Xenogenic demineralized bone matrix and fresh autogenous cortical bone effects on experimental bone healing: Radiological, histopathological and biomechanical evaluation. *Journal of Orthopaedics and Traumatology*, *9*, 73–80. <https://doi.org/10.1007/s10195-008-0006-6>
- Chaya, A., Yoshizawa, S., Verdels, K., Myers, N., Costello, B. J., Chou, D. T., ... Sfeir, C. (2015). In vivo study of magnesium plate and screw degradation and bone fracture healing. *Acta Biomaterialia*, *18*, 262–269. <https://doi.org/10.1016/j.actbio.2015.02.010>
- Chaya, A., Yoshizawa, S., Verdels, K., Noorani, S., Costello, B. J., & Sfeir, C. (2015). Fracture healing using degradable magnesium fixation plates and screws. *Journal of Oral and Maxillofacial Surgery*, *73*, 295–305. <https://doi.org/10.1016/j.joms.2014.09.007>
- Chen, Y., Zhao, S., Liu, B., Chen, M., Mao, J., He, H., ... Wan, G. (2014). Corrosion-controlling and osteo-compatible Mg ion-integrated phytic acid (Mg-PA) coating on magnesium substrate for biodegradable implants application. *ACS Applied Materials & Interfaces*, *6*, 19531–19543. <https://doi.org/10.1021/am506741d>
- Cuthbert, R. J., Churchman, S. M., Tan, H. B., McGonagle, D., Jones, E., & Giannoudis, P. V. (2013). Induced periosteum a complex cellular scaffold for the treatment of large bone defects. *Bone*, *57*, 484–492. <https://doi.org/10.1016/j.bone.2013.08.009>
- Deng, L., Li, D., Yang, Z., Xie, X., & Kang, P. (2017). Repair of the calvarial defect in goat model using magnesium-doped porous hydroxyapatite combined with recombinant human bone morphogenetic protein-2. *Biomedical Materials and Engineering*, *28*, 361–377. <https://doi.org/10.3233/BME-171678>
- Dimitriou, R., Mataliotakis, G. I., Calori, G. M., & Giannoudis, P. V. (2012). The role of barrier membranes for guided bone regeneration and restoration of large bone defects: Current experimental and clinical evidence. *BMC Medicine*, *10*, 81. <https://doi.org/10.1186/1741-7015-10-81>
- Ding, X., Wei, X., Huang, Y., Guan, C., Zou, T., Wang, S., ... Fan, Y. (2015). Delivery of demineralized bone matrix powder using a salt-leached silk fibroin carrier for bone regeneration. *Journal of Materials Chemistry B*, *3*, 3177–3188. <https://doi.org/10.1039/C5TB00046G>
- D'Mello, S., Elangovan, S., Hong, L., Ross, R. D., Sumner, D. R., & Salem, A. K. (2015). Incorporation of copper into chitosan scaffolds promotes bone regeneration in rat calvarial defects. *Journal of Biomedical Materials Research Part B Applied Biomaterials*, *103*, 1044–1049. <https://doi.org/10.1002/jbm.b.33290>
- Dozza, B., Lesci, I. G., Duchi, S., Bella, E. D., Martini, L., Salamanna, F., ... Donati, D. (2017). When size matters: Differences in demineralized bone matrix particles affect collagen structure, mesenchymal stem cell behavior, and osteogenic potential. *Journal of Biomedical Materials Research Part a*, *105*, 1019–1033. <https://doi.org/10.1002/jbm.a.35975>
- Dziuba, D., Meyer-Lindenberg, A., Seitz, J. M., Waizy, H., Angrisani, N., & Reifenrath, J. (2013). Long-term in vivo degradation behaviour and biocompatibility of the magnesium alloy ZEK100 for use as a biodegradable bone implant. *Acta Biomaterialia*, *9*, 8548–8560. <https://doi.org/10.1016/j.actbio.2012.08.028>
- El-Rashidy, A. A., Roether, J. A., Harhaus, L., Kneser, U., & Boccaccini, A. R. (2017). Regenerating bone with bioactive glass scaffolds: A review of in vivo studies in bone defect models. *Acta Biomaterialia*, *62*, 1–28. <https://doi.org/10.1016/j.actbio.2017.08.030>
- Epstein, N. E. (2013). Complications due to the use of BMP/INFUSE in spine surgery: The evidence continues to mount. *Surgery Neurology International*, *4*, S343–S352. <https://doi.org/10.4103/2152-7806.114813>
- Fan, J., Im, C. S., Cui, Z. K., Guo, M., Bezouglaia, O., Fartash, A., ... Aghaloo, T. (2015). Delivery of phenamil enhances BMP-2-induced osteogenic differentiation of adipose-derived stem cells and bone formation in calvarial defects. *Tissue Engineering Part a*, *21*, 2053–2065. <https://doi.org/10.1089/ten.tea.2014.0489>
- Fischer, J., Prosenc, M. H., Wolff, M., Hort, N., Willumeit, R., & Feyerabend, F. (2010). Interference of magnesium corrosion with tetrazolium-based cytotoxicity assays. *Acta Biomaterialia*, *6*, 1813–1823. <https://doi.org/10.1016/j.actbio.2009.10.020>
- Fujihara, K., Kotaki, M., & Ramakrishna, S. (2005). Guided bone regeneration membrane made of polycaprolactone/calcium carbonate composite nano-fibers. *Biomaterials*, *26*, 4139–4147. <https://doi.org/10.1016/j.biomaterials.2004.09.014>
- Gentile, P., Chiono, V., Carmagnola, I., & Hatton, P. V. (2014). An overview of poly (lactic-co-glycolic) acid (PLGA)-based biomaterials for bone tissue engineering. *International Journal of Molecular Sciences*, *15*, 3640–3659. <https://doi.org/10.3390/ijms15033640>
- Govender, S., Csimma, C., Genant, H. K., Opan, A. V., Amit, Y., Arbel, R., ... Börner, M. G. (2002). Recombinant human bone morphogenetic protein-2 for treatment of open tibial fractures: A prospective, controlled, randomized study of four hundred and fifty patients. *The Journal of Bone & Joint Surgery*, *84*, 2123–2134.
- Gruskin, E., Doll, B. A., Futrell, F. W., Schmitz, J. P., & Hollinger, J. O. (2012). Demineralized bone matrix in bone repair: History and use. *Advanced Drug Delivery Reviews*, *64*, 1063–1077. <https://doi.org/10.1016/j.addr.2012.06.008>
- Han, P., Cheng, P., Zhang, S., Zhao, C., Ni, J., Zhang, Y., ... Zheng, Y. (2015). In vitro and in vivo studies on the degradation of high-purity Mg (99.99 wt.%) screw with femoral intracondylar fractured rabbit model. *Biomaterials*, *64*, 57–69. <https://doi.org/10.1016/j.biomaterials.2015.06.031>
- Henkel, J., Woodruff, M. A., Epari, D. R., Steck, R., Glatt, V., Dickinson, I. C., ... Hutmacher, D. W. (2013). Bone regeneration based on tissue engineering conceptions – A 21st century perspective. *Bone Reserch*, *1*, 216–248. <https://doi.org/10.4248/BR201303002>
- Hoffer, M. J., Griffon, D. J., Schaeffer, D. J., Johnson, A. L., & Thomas, M. W. (2008). Clinical applications of demineralized bone matrix: A retrospective and case-matched study of seventy-five dogs. *Veterinary Surgery*, *37*, 639–647. <https://doi.org/10.1111/j.1532-950X.2008.00430.x>
- Hokugo, A., Saito, T., Li, A., Sato, K., Tabata, Y., & Jarrahy, R. (2004). Stimulation of bone regeneration following the controlled release of water-insoluble oxysterol from biodegradable hydrogel. *Biomaterials*, *35*, 5565–5571. <https://doi.org/10.1016/j.biomaterials.2014.03.018>

- Holzwarth, J. M., & Ma, J. M. (2011). Biomimetic nanofibrous scaffolds for bone tissue engineering. *Biomaterials*, 32, 9622–9629. <https://doi.org/10.1016/j.biomaterials.2011.09.009>
- Huang, K. C., Yano, F., Murahashi, Y., Takano, S., Kitaura, Y., Chang, S. H., ... Shihara, K. (2017). Sandwich-type PLLA-nanosheets loaded with BMP-2 induce bone regeneration in critical-sized mouse calvarial defects. *Acta Biomaterialia*, 59, 12–20. <https://doi.org/10.1016/j.actbio.2017.06.041>
- Inzana, J. A., Olvera, D., Fuller, S. M., Kelly, J. P., Graeve, O. A., Schwarz, E. M., ... Awad, H. A. (2014). 3D printing of composite calcium phosphate and collagen scaffolds for bone regeneration. *Biomaterials*, 35, 4026–4034. <https://doi.org/10.1016/j.biomaterials.2014.01.064>
- James, A. W., LaChaud, G., Shen, J., Asatrian, G., Nguyen, V., Zhang, X., ... Soo, C. (2016). A review of the clinical side effects of bone morphogenetic protein-2. *Tissue Engineering Part B: Reviews*, 22, 284–297. <https://doi.org/10.1089/ten.teb.2015.0357>
- Kawata, M., Azuma, K., Izawa, H., Morimoto, M., Saimoto, H., & Ifuku, S. (2016). Biomimetic mineralization of calcium phosphate crystals on chitin nanofiber hydrogel for bone regeneration material. *Carbohydrate Polymers*, 136, 964–969. <https://doi.org/10.1016/j.carbpol.2015.10.009>
- Khoshzaban, A., Mehrzad, S., Tavakoli, V., Keshel, S. H., Behrouzi, G. R., & Bashtar, M. (2011). The comparative effectiveness of demineralized bone matrix, beta-tricalcium phosphate, and bovine-derived anorganic bone matrix on inflammation and bone formation using a paired calvarial defect model in rats. *Clinical, Cosmetic and Investigational Dentistry*, 3, 69–78. <https://doi.org/10.2147/CCIDEN.S13115>
- Kim, J. A., Lim, J., Naren, R., Yun, H. S., & Park, E. K. (2016). Effect of the biodegradation rate controlled by pore structures in magnesium phosphate ceramic scaffolds on bone tissue regeneration in vivo. *Acta Biomaterialia*, 44, 155–167. <https://doi.org/10.1016/j.actbio.2016.08.039>
- Kinney, R. C., Ziran, B. H., Hirshorn, K., Schlatterer, D., & Ganey, T. (2010). Demineralized bone matrix for fracture healing: Fact or fiction? *Journal Orthopaedic Trauma*, 24, S52–S55. <https://doi.org/10.1097/BOT.0b013e3181d07ffa>
- Lee, J., Perikamana, S. K. M., Ahmad, T., Lee, M. S., Yang, H. S., Kim, D. G., ... Shin, H. (2017). Controlled retention of BMP-2-derived peptide on nanofibers based on mussel-inspired adhesion for bone formation. *Tissue Engineering Part a*, 23, 323–334. <https://doi.org/10.1089/ten.tea.2016.0363>
- Li, B., Wang, L., Hao, Y., Wei, D., Li, Y., Feng, Y., ... Zhou, Y. (2015). Ultra-violet-crosslinkable and injectable chitosan/hydroxyapatite hybrid hydrogel for critical size calvarial defect repair in vivo. *Journal of Nanotechnology in Engineering and Medicine*, 6, 041001. <https://doi.org/10.1115/1.4032902>
- Li, L., Zhou, G., Wang, Y., Yang, G., Ding, S., & Zhou, S. (2015). Controlled dual delivery of BMP-2 and dexamethasone by nanoparticle-embedded electrospun nanofibers for the efficient repair of critical-sized rat calvarial defect. *Biomaterials*, 37, 218–229. <https://doi.org/10.1016/j.biomaterials.2014.10.015>
- Li, X., Chu, C., Liu, L., Liu, X., Bai, J., Guo, C., ... Chu, P. K. (2015). Biodegradable poly-lactic acid based-composite reinforced unidirectionally with high-strength magnesium alloy wires. *Biomaterials*, 49, 135–144. <https://doi.org/10.1016/j.biomaterials.2015.01.060>
- Li, X., Qi, C., Han, L., Chu, C., Bai, J., Guo, C., ... Chu, P. K. (2017). Influence of dynamic compressive loading on the in vitro degradation behavior of pure PLA and Mg/PLA composite. *Acta Biomaterialia*, 64, 269–278. <https://doi.org/10.1016/j.actbio.2017.08.004>
- Liu, A., Sun, M., Shao, H., Yang, X., Ma, C., He, D., ... Xu, S. (2016). The outstanding mechanical response and bone regeneration capacity of robocast dilute magnesium-doped wollastonite scaffolds in critical size bone defects. *Journal of Materials Chemistry B*, 4, 3945–3958. <https://doi.org/10.1039/C6TB00449K>
- Lu, J., Cheng, C., He, Y. S., Lyu, C., Wang, Y., Yu, J., ... Li, D. (2016). Multi-layered graphene hydrogel membranes for guided bone regeneration. *Advanced Materials*, 28, 4025–4031. <https://doi.org/10.1002/adma.201505375>
- Ma, R., Lai, Y. X., Li, L., Tan, H. I., Wang, J. L., Li, Y., ... Qin, L. (2015). Bacterial inhibition potential of 3D rapid-prototyped magnesium-based porous composite scaffolds: An in vitro efficacy study. *Scientific Reports*, 5, 13775. <https://doi.org/10.1038/srep13775>
- Maddox, E., Zhan, M., Mundy, G. R., Drohan, W. N., & Burgess, W. H. (2004). Optimizing human demineralized bone matrix for clinical application. *Tissue Engineering*, 6, 441–448. <https://doi.org/10.1089/107632700418146>
- Mouri o, V., Cattalini, J. P., & Boccaccini, A. R. (2012). Metallic ions as therapeutic agents in tissue engineering scaffolds: An overview of their biological applications and strategies for new developments. *Journal of the Royal Society Interface*, 9, 401–419. <https://doi.org/10.1098/rsif.2011.0611>
- Nommeots-Nomm, A., Labbaf, S., Devlin, A., Todd, N., Geng, H., Solanki, A. K., ... Ejeian, F. (2017). Highly degradable porous melt-derived bioactive glass foam scaffolds for bone regeneration. *Acta Biomaterialia*, 57, 449–461. <https://doi.org/10.1016/j.actbio.2017.04.030>
- Rhee, S. C., Ji, Y. H., Gharibjanian, N. A., Dhong, E. S., Park, S. H., & Yoon, E. S. (2011). In vivo evaluation of mixtures of uncultured freshly isolated adipose-derived stem cells and demineralized bone matrix for bone regeneration in a rat critically sized calvarial defect model. *Stem Cells and Development*, 20, 233–242. <https://doi.org/10.1089/scd.2009.0525>
- Seo, B. B., Koh, J. T., & Song, S. C. (2017). Tuning physical properties and BMP-2 release rates of injectable hydrogel systems for an optimal bone regeneration effect. *Biomaterials*, 122, 91–104. <https://doi.org/10.1016/j.biomaterials.2017.01.016>
- Shanov, V. N., Chaudhury, P. R., Schulz, M. J., Yin, Z., Naciff, B. C., & Wang, Y. (2017). Methods for making magnesium biodegradable stents for medical implant applications. *US Patent*, 9, 655.
- Shi, L., Wang, F., Zhu, W., Xu, Z., Fuchs, S., Hilborn, J., ... Weng, X. (2017). Self-healing silk fibroin-based hydrogel for bone regeneration: Dynamic metal-ligand self-assembly approach. *Advanced Functional Materials*, 27, 1700591. <https://doi.org/10.1002/adfm.201700591>
- Shi, Y. J., Pei, J., Zhang, J., Niu, J. I., Zhang, H., Guo, S. R., ... Yuan, G. Y. (2017). Enhanced corrosion resistance and cytocompatibility of biodegradable Mg alloys by introduction of Mg(OH)₂ particles into poly(L-lactic acid) coating. *Scientific Reports*, 7, 41796. <https://doi.org/10.1038/srep41796>
- Shin, S. H., Purevdorj, O., Castano, O., Planell, J. A., & Kim, H. W. (2012). A short review: Recent advances in electrospinning for bone tissue regeneration. *Journal Tissue Engineering*, 3, 1041731412443530. <https://doi.org/10.1177/2041731412443530>
- Spicer, P. P., Kretlow, J. D., Young, S., Jansen, J. A., Kasper, F. K., & Mikos, A. G. (2012). Evaluation of bone regeneration using the rat critical size calvarial defect. *Nature Protocols*, 7, 1918–1928. <https://doi.org/10.1038/nprot.2012.113>
- Stancoven, B. W., Lee, J., Dixon, D. R., Iii, M. P., Bisch, F. C., Wikesjö, U. M. E., & Susin, C. (2013). Effect of bone morphogenetic protein-2, demineralized bone matrix and systemic parathyroid hormone (1-34) on local bone formation in a rat calvaria critical-size defect model. *Journal of Periodontal Research*, 48, 243–251. <https://doi.org/10.1111/jre.12001>
- Sun, M., Liu, A., Shao, H., Yang, X., Ma, C., Yan, S., ... Gou, Z. (2016). Systematical evaluation of mechanically strong 3D printed diluted magnesium doping wollastonite scaffolds on osteogenic capacity in rabbit calvarial defects. *Scientific Reports*, 6, 34029. <https://doi.org/10.1038/srep34029>
- Temenoff, J. S., & Mikos, A. G. (2008). *Biomaterials: The intersection of biology and materials science*. Upper Saddle River, N.J.: Pearson/Prentice Hall.
- Townsend, J. M., Dennis, S. C., Whitlow, J., Feng, Y., Wang, J., Andrews, B., ... Berkland, C. J. (2017). Colloidal gels with extracellular matrix particles and growth factors for bone regeneration in critical size rat calvarial defects. *The AAPS Journal*, 19, 703–711. <https://doi.org/10.1208/s12248-017-0045-0>

- Valentin-Opran, A., Wozney, J., Csimma, C., Lilly, L., & Riedel, G. E. (2002). Clinical evaluation of recombinant human bone morphogenetic protein-2. *Clinical Orthopaedics & Related Research*, 395, 110–120.
- Van Houdt, C. I. A., Cardoso, D. A., Van Oirschot, B., Ulrich, D. J. O., Jansen, J. A., Leeuwenburgh, S. C. G., & Van den Beucken, J. (2017). Porous titanium scaffolds with injectable hyaluronic acid-DBM gel for bone substitution in a rat critical-sized calvarial defect model. *Journal of Tissue Engineering Regenerative Medicine*, 11, 2537–2548. <https://doi.org/10.1002/term.2151>
- Wang, J., & Glimcher, M. J. (1999). Characterization of matrix-induced osteogenesis in rat calvarial bone defects: I. Differences in the cellular response to demineralized bone matrix implanted in calvarial defects and in subcutaneous sites. *Calcified Tissue International*, 65, 156–165. <https://doi.org/10.1007/s002239900676>
- Wang, J., Liu, L., Wu, Y., Maitz, M. F., Wang, Z., Koo, Y., ... Yun, Y. (2017). Ex vivo blood vessel bioreactor for analysis of the biodegradation of magnesium stent models with and without vessel wall integration. *Acta Biomaterialia*, 50, 546–555. <https://doi.org/10.1016/j.actbio.2015.04.011>
- Wang, J., Witte, F., Xi, T., Zheng, Y., Yang, K., Yang, Y., ... Qin, L. (2015). Recommendation for modifying current cytotoxicity testing standards for biodegradable magnesium-based materials. *Acta Biomaterialia*, 21, 237–249. <https://doi.org/10.1016/j.actbio.2015.04.011>
- Wang, Z., Lin, M., Xie, Q., Sun, H., Huang, Y., Zhang, D., ... Wang, J. (2016). Electrospun silk fibroin/poly (lactide-co-ε-caprolactone) nanofibrous scaffolds for bone regeneration. *International Journal of Nanomedicine*, 11, 1483–1500. <https://doi.org/10.2147/IJN.S97445>
- Wang, Z., Wang, K., Lu, X., Li, M., Liu, H., Xie, C., ... Zhi, W. (2015). BMP-2 encapsulated polysaccharide nanoparticle modified biphasic calcium phosphate scaffolds for bone tissue regeneration. *Journal of Biomedical Materials Research Part A*, 103, 1520–1532. <https://doi.org/10.1002/jbm.a.35282>
- Wen, W., Zou, Z., Luo, B., & Zhou, C. (2017). In vitro degradation and cytocompatibility of g-MgO whiskers/PLLA composites. *Journal of Materials Science*, 52, 2329–2344. <https://doi.org/10.1007/s10853-016-0525-0>
- Wildemann, B., Kadow-Romacker, A., Haas, N. P., & Schmidmaier, G. (2010). Quantification of various growth factors in different demineralized bone matrix preparations. *Journal of Biomedical Materials Research Part A*, 81A, 437–442. <https://doi.org/10.1002/jbm.a.31085>
- Willbold, E., Gu, X., Albert, D., Kalla, K., Bobe, K., Brauneis, M., ... Tillmann, W. (2015). Effect of the addition of low rare earth elements (lanthanum, neodymium, cerium) on the biodegradation and biocompatibility of magnesium. *Acta Biomaterialia*, 11, 554–562. <https://doi.org/10.1016/j.actbio.2014.09.041>
- Witte, F. (2015). Reprint of: The history of biodegradable magnesium implants: A review. *Acta Biomaterialia*, 23, S28–S40. <https://doi.org/10.1016/j.actbio.2015.07.017>
- Wongsupa, N., Nuntanarant, T., Kamolmattayakul, S., & Thuaksuban, N. (2017). Assessment of bone regeneration of a tissue-engineered bone complex using human dental pulp stem cells/poly (ε-caprolactone)-biphasic calcium phosphate scaffold constructs in rabbit calvarial defects. *Journal of Materials Science: Materials in Medicine*, 28, 77. <https://doi.org/10.1007/s10856-017-5883-x>
- Wu, G., Ibrahim, J. M., & Chu, P. K. (2013). Surface design of biodegradable magnesium alloys – A review. *Surface and Coating Technology*, 233, 2–12. <https://doi.org/10.1016/j.surfcoat.2012.10.009>
- Wu, Y., Li, N., Cheng, Y., Zheng, Y., & Han, Y. (2013). In vitro study on biodegradable AZ31 magnesium alloy fibers reinforced PLGA composite. *Journal of Materials Science Technology*, 29, 545–550. <https://doi.org/10.1016/j.jmst.2013.03.004>
- Xu, T. O., Kim, H. S., Stahl, T., & Nukavarapu, S. P. (2018). Self-neutralizing PLGA/magnesium composites as novel biomaterials for tissue engineering. *Biomedical Materials*. <https://doi.org/10.1088/1748-605X/aaaa29>
- Yao, Q., Cosme, J. G., Xu, T., Miszuk, J. M., Picciani, P. H., Fong, H., & Sun, H. (2017). Three dimensional electrospun PCL/PLA blend nanofibrous scaffolds with significantly improved stem cells osteogenic differentiation and cranial bone formation. *Biomaterials*, 115, 115–127. <https://doi.org/10.1016/j.biomaterials.2016.11.018>
- Yassin, M. A., Mustafa, K., Xing, Z., Sun, Y., Fasmer, K. E., Waag, T., ... Leknes, K. N. (2017). A copolymer scaffold functionalized with nanodiamond particles enhances osteogenic metabolic activity and bone regeneration. *Macromolecular Bioscience*, 17, 1600427. <https://doi.org/10.1002/mabi.201600427>
- Yu, H. J., Wang, J. Q., Shi, X. T., Louzguine-Luzgin, D. V., Wu, H. K., & Perepezko, J. H. (2013). Ductile biodegradable Mg-based metallic glasses with excellent biocompatibility. *Advanced Functional Materials*, 23, 4793–4800. <https://doi.org/10.1002/adfm.201203738>
- Zhang, J., Liu, H., Ding, J. X., Wu, J., Zhuang, X. L., Chen, X. S., ... Li, Z. M. (2016). High-pressure compression-molded porous resorbable polymer/hydroxyapatite composite scaffold for cranial bone regeneration. *ACS Biomaterials Science & Engineering*, 2, 1471–1482. <https://doi.org/10.1021/acsbomaterials.6b00202>
- Zhang, J., Ma, X., Lin, D., Shi, H., Yuan, Y., Tang, W., ... Liu, C. (2015). Magnesium modification of a calcium phosphate cement alters bone marrow stromal cell behavior via an integrin-mediated mechanism. *Biomaterials*, 53, 251–264. <https://doi.org/10.1016/j.biomaterials.2015.02.097>
- Zhang, S., Guo, Y., Dong, Y., Wu, Y., Cheng, Y., Wang, Y., ... Yuan, Q. (2016). A novel nanosilver/nanosilica hydrogel for bone regeneration in infected bone defects. *ACS Applied Materials & Interfaces*, 8, 13242–13250. <https://doi.org/10.1021/acsam.6b01432>
- Zhang, X., Zhang, C., Lin, Y., Hu, P., Shen, Y., Wang, K., ... Liu, X. (2016). Nanocomposite membranes enhance bone regeneration through restoring physiological electric microenvironment. *ACS Nano*, 10, 7279–7286. <https://doi.org/10.1021/acsnano.6b02247>
- Zhang, Y., Xu, J., Ruan, Y. C., Yu, M. K., O'Laughlin, M., Wise, H., ... Qin, L. (2016). Implant-derived magnesium induces local neuronal production of CGRP to improve bone-fracture healing in rats. *Nature Medicine*, 22, 1160–1169. <https://doi.org/10.1038/nm.4162>
- Zhao, D., Witte, F., Lu, F., Wang, J., Li, J., & Qin, L. (2017). Current status on clinical applications of magnesium-based orthopaedic implants: A review from clinical translational perspective. *Biomaterials*, 112, 287–302. <https://doi.org/10.1016/j.biomaterials.2016.10.017>
- Zheng, Y. F., Gu, X. N., & Witte, F. (2014). Biodegradable metals. *Materials Science and Engineering: R: Reports*, 77, 1–34. <https://doi.org/10.1016/j.mser.2014.01.001>
- Zhu, Y., Li, D., Zhang, K., Jiang, L., Shi, C., Fangteng, J., ... Sun, H. (2017). Novel synthesized nanofibrous scaffold efficiently delivered hBMP-2 encoded in adenoviral vector to promote bone regeneration. *Journal of Biomedical Nanotechnology*, 13, 437–446. <https://doi.org/10.1166/jbn.2017.2361>
- Zhu, Y., Mao, Z., & Gao, C. (2013). Control over the gradient differentiation of rat BMSCs on a PCL membrane with surface-immobilized alendronate gradient. *Biomacromolecules*, 14, 342–349. <https://doi.org/10.1021/bm301523p>
- Zweiben, C., Smith, W., Wardle, M. (1979). Test methods for fiber tensile strength, composite flexural modulus, and properties of fabric-reinforced laminates. *Composite Materials: Testing and Design (Fifth Conference)*, ASTM International. <https://doi.org/10.1520/STP369125>

SUPPORTING INFORMATION

Additional supporting information may be found online in the Supporting Information section at the end of the article.

Figure S1 (a) SEM images of BMSCs cultured on TCPS, PLGA@HA, PLGA@HA&DBM, and Mg-PLGA@HA&DBM for 7 days, and (b)

in vitro cell viability of BMSCs seeded on scaffolds for 1, 3 and 7 days (* $p < 0.05$).

Figure S2 Micro-CT images of scaffolds after implantation in a critical-sized calvarial defect for 12 weeks. The solid calcification area was noticeable along with Mg struts in Mg-PLGA@HA and Mg-PLGA@HA&DBM samples.

How to cite this article: Chen Y, Ye S-H, Sato H, et al. Hybrid scaffolds of Mg alloy mesh reinforced polymer/extracellular matrix composite for critical-sized calvarial defect reconstruction. *J Tissue Eng Regen Med.* 2018;12:1374–1388. <https://doi.org/10.1002/term.2668>